Available online at www.sciencedirect.com
SCIENCE DIRECT®
Solar Energy 76 (2004) 623–633
SOLAR ENERGY
www.elsevier.com/locate/solener

Numerical and experimental analysis of convection heat transfer in passive solar heating room with greenhouse and heat storage

Wei Chen, Wei Liu *

School of Energy and Power Engineering, Huazhong University of Science and Technology, Wuhan, Hubei 430074, PR China

Received 18 March 2003; received in revised form 14 November 2003; accepted 17 November 2003

Communicated by: Associate Editor Gabriela Alvarez-Garcia

Abstract

In this paper, heat transfer and air flow in passive solar heating room with greenhouse and heat storage are studied. Thermal insulation of solar heating room has significant effects on temperature distribution and airflow in the heating chamber of this solar system. Heat transfer and air flow in a rock bed, which is used as solar absorber and storage layer, are also studied. If porosity is kept within certain range, increasing the rock size causes an increase of the capability of thermal storage and heating effects; increasing the porosity of thermal storage materials results in an increase of the bed temperature but a decrease of the rock mass. The specific heat capacity and thermal conductivity have a remarkable effect on the average temperature of rock bed. All these factors should be taken into account when designing a solar heating system.

Keywords: Greenhouse; Heat storage; Solar heating

1. Introduction

Passive solar heating is widely used in the cold climates. Many passive heating techniques, such as trombe wall, transparent insulation etc., are used in the building design (Nisbet and Kwan, 1987; Yang et al., 2000; Athienitis, 1997; Raman and Mande, 2001). Earlier studies show that the passive solar heating room with greenhouse and heat storage works well in winter (Dickinson and Anderson, 1980), in which the energy storage is an essential for the solar heating system. Solar radiation is a time-dependent energy source and of intermittent character. More energy than necessary is usually available when the sun is shining. This extra energy is first stored then used when the sun is not shining. Rock bed is generally used as an air-based thermal energy storage system. The performance of heat storage in a rock bed is influenced by various design and operational parameters such as size of rock and bed, air mass flow rate, void fraction within rock bed, thermal and physical properties of rock. Although many scientists have studied the performance and the design methods for the device of rock-bed energy storage (Robinson and Dorenkamp, 1977; Chandra and Willits, 1981; Coutier and Farber, 1982; Choudhury et al., 1995), most designs for the thermal storage system just focus on fluid transport system, heat exchanger, control system, collector, valve, pump, expansion tank and heat storage container, etc.

In the present work, a special structure in solar heating system is studied, which works as an absorber with the function of heat storage, to reduce the cost of system. The performance of heat storage in the passive

* Corresponding author. Tel.: +86-27-8754-2618; fax: +86-27-8754-0724.

E-mail addresses: weichen96@sina.com (W. Chen), w_liu@nxu.edu.cn (W. Liu).

0038-092X/$ - see front matter © 2003 Elsevier Ltd. All rights reserved.
doi:10.1016/j.solener.2003.11.006

Nomenclature

A_r	surface area of the thermal storage layer on the side of the greenhouse in the heating system, m^2
A_w	surface area of the partition wall on the side of the greenhouse in the heating system, m^2
c	specific heat, J/(kg K)
c_1	constant for the turbulence model
c_2	constant for the turbulence model
c_μ	constant for the turbulence model
C	inertia coefficient, defined in Eq. (10)
d	diameter, m
f_1	turbulence model coefficient
f_2	turbulence model coefficient
f_μ	turbulence model coefficient
g	gravitational acceleration vector, m/s^2
G	turbulence model coefficient
G_{gsun}	rate of solar flux absorbed by the glass enclosure of the greenhouse, W/m^2
G_{rsun}	rate of solar flux absorbed by the rock bed surface in the greenhouse, W/m^2
G_{wsun}	rate of solar flux absorbed by the partition wall surface on the side of greenhouse in the heating system, W/m^2
h_r	thickness of rock bed, m
k_f	fluid thermal conductivity, W/(m K)
k_m	apparent thermal conductivity, W/(m K)
k_s	rock thermal conductivity, W/(m K)
k_w	thermal conductivity for the partition wall absorber, W/(m K)
k	turbulence kinetic energy
K	permeability of the rock bed, m^2
P	pressure, Pa
Q_{ai}	convective heat exchange between the air inside heating system and the enclosure of greenhouse except the surface of partition wall, J
Q_{ao}	convective heat exchange between the ambient and the glass enclosure of greenhouse except the surface of partition wall, J
Q_{ar}	convective heat exchange between the air inside heating system and the surface of rock bed, J
Q_{aw}	convective heat exchange between the air inside heating system and the surface of partition wall absorber in the greenhouse, J
Q_{hg}	thermal radiation exchange of the glass enclosure with the surfaces of rock bed and partition wall inside the greenhouse, J
Q_{hr}	thermal radiation exchange of the rock bed surface with the glass enclosure and the partition wall inside the greenhouse, J
Q_{hw}	thermal radiation exchange of the partition wall absorber surface with the surface of rock bed and the glass enclosure in the greenhouse, J
Q_{sky}	thermal radiation exchange between the glass enclosure and the sky, J
Re	Reynolds number
S	source term
T	temperature, K(°C)
T_{ao}	ambient temperature, K(°C)
u	velocity component in x-direction, m/s
$\lvert\vec{v}_d\rvert$	mean velocity($=\sqrt{u_d^2+v_d^2}$), m/s
v	velocity component in y-direction, m/s
V	volume, m^3
x	horizontal coordinate, m
y	vertical coordinate, m

Greek symbols

β	thermal expansion coefficient, 1/K
τ	time, s
Γ	exchange coefficient
ε	dissipation rate of turbulent kinetic
σ_ε	constant for the turbulence model
σ_k	constant for the turbulence model
σ_t	constant for the turbulence model
μ	dynamic viscosity, kg/(m s)
μ_{efft}	effective dynamic viscosity for turbulence model, kg/(m s)
ρ	density, kg/m^3
ϕ	dependent variable
θ	porosity of porous medium, %

Subscripts

a	air
c	cold wall
d	Darcy
eff	effective
f	fluid in rock bed
g	glass plate or roof
p	pebble
r	rock
m	apparent mean
s	solid for rock bed
t	turbulent
w	partition wall on the side of greenhouse

Superscript

–	average

solar heating room with a greenhouse, influenced by size, void fraction and material of the rock bed, is analyzed. The effects of wall thermal insulation of a solar heating room on the temperature distribution and the

gas flow in the solar system are explored. The main objective of the present study focuses on the strategies to save more energy at lower cost and maintain thermal comfort inside the building in cold climates.

2. System description and mathematical analysis

2.1. System description

The passive solar heating room with a greenhouse and a heat storage layer under investigation is shown schematically in Fig. 1. The system consists of a greenhouse and a heating room. The greenhouse is designed to directly gain solar heat. It has a thermal storage wall with a top and a bottom vent and an inclined roof facing the south. The south wall of the heating room has two functions, one as a solar absorber on the side of the greenhouse, the other as an insulator on the side of the heating room. The rock bed as a solar absorber and a storage layer locates at the bottom of the greenhouse, and extends to the heating room. The roof and wall of greenhouse except the partition wall are made of glass.

2.2. Thermal analysis

A thermal analysis has been conducted to determine system performance in terms of radiation, convection and conduction. The heat transfer process can be expressed as follows.

The convection heat exchange between the air and the glass enclosure of greenhouse is:

$$Q_a = Ah(T_a - T_e) \tag{1}$$

where T_e is the temperature of glass enclosure. The heat convection coefficient h is calculated by using appropriate relations in the literature (Duffie and Beckman, 1980).

The radiation heat exchange among N grey surfaces that form an enclosure can be written for the surface i (Chen, 1990) as:

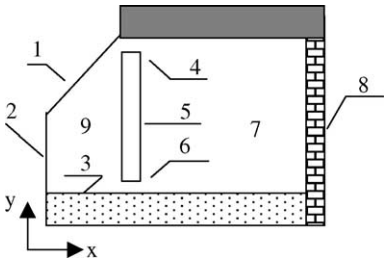

Fig. 1. Schematic of a passive solar heating system with a greenhouse and a heat storage layer. 1—greenhouse roof; 2—glass wall of greenhouse; 3—heat storage layer; 4—top vent; 5—partition wall; 6—bottom vent; 7—heating room; 8—north wall; 9—greenhouse.

$$J_i = \varepsilon_i \sigma T_i^4 + (1 - \varepsilon_i) \sum_j^N J_j F_{i,j} \tag{2}$$

$$Q_{hi} = \left(\sigma T_i^4 - \sum_j^N F_{i,j} J_j \right) \varepsilon_i A_i \tag{3}$$

where J is radiation, ε_i is emissivity of the surface i, σ is Stefan–Boltzman constant, $F_{i,j}$ is view factors between surfaces i and j, subscripts i, j refer to the surface i, j.

The energy equilibrium equations for the different components of the passive solar heating system with its greenhouse and heat storage layer can be established according to the following assumptions.

(1) The air temperature in the heating room and the greenhouse is uniform.
(2) No temperature gradient exists on the glass surfaces of greenhouse, and on the surfaces of heat storage layer and partition wall of the heating system.
(3) All surfaces of heat storage layer, partition wall, glass enclosure and roof in the greenhouse are considered as the grey bodies.
(4) The enclosure, including the partition wall of the heating room and the wall and roof of heating room, is considered as the thermally insulated.

The transient energy equations are given in the way of node method, from which we can obtain the transient temperatures. The equations simply reduce to the balance equations when $\tau \to \infty$, from which we can obtain the boundary temperatures of the system.

For the air in the solar heating system:

$$\rho_a c_a V_a \frac{dT_a}{d\tau} = Q_{ar} + Q_{aw} + Q_{ai} \tag{4}$$

For the glass plate or roof in greenhouse:

$$\rho_g c_g V_g \frac{dT_g}{d\tau} = G_{gsun} + Q_{sky} + Q_{ai} + Q_{ao} + Q_{hg} \tag{5}$$

For the thermal storage layer in greenhouse:

$$\rho_r c_r V_r \frac{dT_r}{d\tau} = G_{rsun} A_r + Q_{hr} + Q_{ar} \tag{6}$$

For the partition wall in greenhouse:

$$\rho_w c_w V_w \frac{dT_w}{d\tau} = G_{wsun} A_w + Q_{aw} + Q_{hw} \tag{7}$$

2.3. Theoretical modeling

The mathematical model and the computational method are developed to study the natural convection of incompressible fluids in the heating system where a porous rock layer is laid on the bottom. The flow is

assumed to be two-dimensional and the Boussinesq approximation is used to account for the air density variation.

It is assumed that the rock bed is considered as a fluid-saturated porous medium and the form-drag and boundary effects are significant. Under the circumstances, the governing equations for airflow and heat transfer in the porous rock layer are (Rees, 2002):

Continuity equation

$$\frac{\partial(\rho u_d)}{\partial x}+\frac{\partial(\rho v_d)}{\partial y}=0 \tag{8}$$

Momentum equations

$$\frac{\rho}{\theta}\frac{\partial u_d}{\partial \tau}+\frac{\rho}{\theta}\left(u_d\frac{\partial u_d}{\partial x}+v_d\frac{\partial u_d}{\partial y}\right) =-\frac{\partial p}{\partial x}+\frac{\partial}{\partial x}\left(\mu_{eff}\frac{\partial u_d}{\partial x}\right)+\frac{\partial}{\partial y}\left(\mu_{eff}\frac{\partial u_d}{\partial y}\right)-\frac{\mu u_d}{K} +\frac{\rho C\theta}{\sqrt{K}}|\vec{v}_d|u_d \tag{9}$$

$$\frac{\rho}{\theta}\frac{\partial v_d}{\partial \tau}+\frac{\rho}{\theta}\left(u_d\frac{\partial v_d}{\partial x}+v_d\frac{\partial v_d}{\partial y}\right) =-\frac{\partial p}{\partial x}+\frac{\partial}{\partial x}\left(\mu_{eff}\frac{\partial v_d}{\partial x}\right)+\frac{\partial}{\partial y}\left(\mu_{eff}\frac{\partial v_d}{\partial y}\right)-\frac{\mu v_d}{K} +\frac{\rho C\theta}{\sqrt{K}}|\vec{v}_d|v_d+\rho g\beta(T-T_c) \tag{10}$$

Energy equation

$$(\rho c)_m\frac{\partial T}{\partial \tau}+\rho c\left(u_d\frac{\partial T}{\partial x}+v_d\frac{\partial T}{\partial y}\right) =\frac{\partial}{\partial x}\left(k_{eff}\frac{\partial T}{\partial x}\right)+\frac{\partial}{\partial y}\left(k_{eff}\frac{\partial T}{\partial y}\right) \tag{11}$$

All constants and variables in the above equations are defined in the nomenclature. Eqs. (8)–(11) form the full set of equations used to model the convective flow in the porous media. Eqs. (9) and (10) contain the force balance between viscosity and pressure gradient known as Darcy's law, which are extended by the further inclusion of terms modeling advective inertia, boundary effects (Brinkman correction) and form-drag (Forchheimer inertia). Eq. (10) also contains a term of buoyancy. The values of permeability K and inertia coefficient C in the momentum equations are given for the packed porous bed with rock diameters d_r and porosity θ (Ergun, 1952; Beckermann et al., 1987).

$$K=\frac{d_r^2\theta^3}{175(1-\theta)^2} \tag{12}$$

$$C=\frac{1.75}{\sqrt{175}}\theta^{-3/2} \tag{13}$$

All physical properties of the porous medium are needed in the calculation. It has been found that taking $\mu_{eff}=\mu_f$ in Brinkman's extension provides good agreement with experimental data (Neale and Nader, 1974) and is adopted in the present work. In addition, k_m and $(\rho c)_m$ are calculated by $k_m=\theta k_f+(1-\theta)k_s$ and $(\rho c)_m=\theta(\rho c)_f+(1-\theta)(\rho c)_s$ (Chen and Chen, 1992).

Above the heat storage bed in the heating room and greenhouse, the airflow is considered as turbulent natural convection. The k–ε model of low-Reynolds number for turbulence flow is used, which is an extension of high-Reynolds number model, thus it can reproduce the wall damping of turbulence and can be used across the viscous sub-layer. The equations for mass continuity, velocity components and temperature take the following forms (Iacovides and Raisee, 2001).

Continuity equation

$$\frac{\partial(\rho u)}{\partial x}+\frac{\partial(\rho v)}{\partial y}=0 \tag{14}$$

Momentum equations

$$\frac{\partial(\rho u)}{\partial \tau}+\frac{\partial(\rho uu)}{\partial x}+\frac{\partial(\rho vu)}{\partial y} =\frac{\partial}{\partial x}\left(\mu_{efft}\frac{\partial u}{\partial x}\right)+\frac{\partial}{\partial y}\left(\mu_{efft}\frac{\partial u}{\partial y}\right)+S_u \tag{15}$$

$$\frac{\partial(\rho v)}{\partial \tau}+\frac{\partial(\rho uv)}{\partial x}+\frac{\partial(\rho vv)}{\partial y} =\frac{\partial}{\partial x}\left(\mu_{efft}\frac{\partial v}{\partial x}\right)+\frac{\partial}{\partial y}\left(\mu_{efft}\frac{\partial v}{\partial y}\right)+S_v \tag{16}$$

The source terms in momentum equations are:

$$S_u=-\frac{\partial p}{\partial x}+\frac{\partial}{\partial x}\left(\mu_{efft}\frac{\partial u}{\partial x}\right)+\frac{\partial}{\partial y}\left(\mu_{efft}\frac{\partial v}{\partial x}\right) \tag{17}$$

$$S_v=-\frac{\partial p}{\partial y}+\frac{\partial}{\partial x}\left(\mu_{efft}\frac{\partial u}{\partial y}\right)+\frac{\partial}{\partial y}\left(\mu_{efft}\frac{\partial v}{\partial y}\right) +\rho g\beta(T-T_C) \tag{18}$$

General transported fluid scalar

$$\frac{\partial(\rho\phi)}{\partial \tau}+\frac{\partial(\rho u\phi)}{\partial x}+\frac{\partial(\rho v\phi)}{\partial y} =\frac{\partial}{\partial x}\left(\Gamma_\phi\frac{\partial \phi}{\partial x}\right)+\frac{\partial}{\partial y}\left(\Gamma_\phi\frac{\partial \phi}{\partial y}\right)+S_\phi \tag{19}$$

where Γ_ϕ is the exchange coefficient for the transport of property ϕ which is for T, k and ε. The source terms in the ϕ equations are:

$$S_k = \mu_t G - \rho\varepsilon - 2\mu\left(\frac{\partial k^{1/2}}{\partial y}\right)^2 \tag{20}$$

$$S_\varepsilon = \frac{\varepsilon}{k} c_1 f_1 \mu_t G - c_2 \rho \frac{\varepsilon^2}{k} f_2 + 2\frac{\mu\mu_t}{\rho}\left(\frac{\partial^2 u}{\partial y^2}\right)^2 \tag{21}$$

$$S_T = 0$$

$$G = \frac{\mu_t}{\rho}\left\{2\left[\left(\frac{\partial u}{\partial x}\right)^2 + \left(\frac{\partial v}{\partial y}\right)^2\right] + \left(\frac{\partial u}{\partial y} + \frac{\partial v}{\partial x}\right)^2\right\}$$

The expression for the turbulent viscosity (22) includes the damping function f_μ given by Eq. (23), in which the damping parameter R_t is local Reynolds number of turbulence defined as $R_t = \rho k^2/(\mu\varepsilon)$.

$$\mu_t = \rho c_\mu f_\mu k^2/\varepsilon \tag{22}$$

$$f_\mu = \exp[-3.4/(1 + 0.02R_t)^2] \tag{23}$$

The damping function f_2 in Eq. (21) for the generation rate of ε is determined with respect to decaying, grid-generated turbulence.

$$f_2 = 1 - 0.3\exp(-Re_t^2) \tag{24}$$

The turbulence model contains several constants that were assigned the following values.

$$c_\mu = 0.09, \quad c_1 = 1.44, \quad c_2 = 1.92, \quad \sigma_k = 1,$$
$$\sigma_\varepsilon = 1.3, \quad \sigma_t = 1, \quad f_1 = 1$$

2.4. Boundary and initial conditions

Numerical simulations were performed under the ambient and operative conditions. A typical cold and sunny day of November in Wuhan, China was considered, and the outdoor temperature (Kang, 1992) and the solar radiative variation (Zhang, 1997) were given by Eqs. (25) and (26).

$$T_{ao}(\tau) = \overline{T_{ao}} + T_{ar}\cos\left(\frac{\pi}{12}(\tau - 14)\right) \tag{25}$$

$$G_{sun}(\tau) = \widehat{G}_{sun}\sin\left(\frac{\tau - a}{b - a}\pi\right), \quad a < \tau < b \tag{26}$$

where $\overline{T_{ao}}$ is for average outside temperature of 10 °C; T_{ar} for amplitude temperature of 6 °C; $\widehat{G}_{sun}$ for maximum solar radiation of 350 W/m^2; a for sunrise hour at 6 o'clock in the morning; b for sunset hour at 18 o'clock in the afternoon; τ for time hours.

The fluid in the solar heating system is initially stagnant and at a uniform temperature which is the same as ambient temperature. The initial and boundary conditions for the energy balance equations are given below.

The glass enclosure surface inside the greenhouse: $T = T_{gs}$, $u = 0$, $v = 0$,
the surfaces of thermal storage bed at bottom of the heating system:

$$u\Big|_{y=h_r^-} = u\Big|_{y=h_r^+}, \quad v\Big|_{y=h_r^-} = v\Big|_{y=h_r^+}, \quad p\Big|_{y=h_r^-} = p\Big|_{y=h_r^+},$$
$$\mu_m\left(\frac{\partial u_d}{\partial y} + \frac{\partial v_d}{\partial x}\right)\Big|_{y=h_r^-} = \mu_{eff}\left(\frac{\partial u}{\partial y} + \frac{\partial v}{\partial x}\right)\Big|_{y=h_r^+}$$

$T = T_{h_r}$ (on the side of the greenhouse),
$T\big|_{y=h_r^-} = T\big|_{y=h_r^+}$ (on the side of the heating room).

The partition wall of the system is divided into two parts, one as a solar absorber on the side of greenhouse, the other as an insulator on the side of heating room, so the boundary conditions of the partition wall are given as follows.

The partition wall surface on the side of greenhouse: $T = T_w$, $u = 0$, $v = 0$,
the roof, the partition wall and the north wall of heating room: $\frac{\partial T}{\partial x} = 0$, $\frac{\partial T}{\partial y} = 0$, $u = 0$, $v = 0$,
the bottom of the rock bed: $\frac{\partial T}{\partial y} = 0$, $u = 0$, $v = 0$,
initial conditions: $\tau = 0$ $T = \text{const}$, $u = 0$, $v = 0$.

3. Numerical procedure

For the present study, the governing equations (8)–(11) and (14)–(19) together with the boundary conditions mentioned above were solved with the SIMPLER method (Patankar, 1980), which is validated for various cases (Tao, 2001). The computer code is based on the mathematical formulation discussed earlier. The control-volume formulation utilized in this method ensures continuity of convective and diffusive fluxes as well as overall momentum and energy conservation. The harmonic mean formulation was used to handle abrupt variations in thermal physical properties, such as permeability and thermal conductivity, across the interface, for example, at the porous/fluid layer interface. This ensures the continuity of convective and diffusive flues across the interface without requiring the use of an excessively fine grid structure.

Non-uniform mesh sizes were used for the numerical computation. The grid in vertical direction was uniformly distributed. In horizontal direction, finer mesh sizes were taken within the heat storage layer. To test the grid independence, two different grid sizes, 128×148 and 128×188, had been employed in the present study, but its influence on the calculating results is small. Therefore, a grid of 128×148 had been chosen.

At the outdoor temperature of 10 °C and the solar radiant intensity of 350 W/m^2, steady-state solutions were attempted to draw the isothermals and streamlines

of the system as the rock bed worked as solar absorber and storage layer had been paved at bottom of the heating system. As to the unsteady-state numerical calculations, the time step was concerned and several values of $\Delta\tau$ had been examined. For example, it had been found that the maximum deviation between the results by using $\Delta\tau = 10$ s and $\Delta\tau = 20$ s was only 1.5%. Hence, the time step of $\Delta\tau = 20$ s together with the grid size of 128×148 was used for the unsteady-state numerical calculations in this study.

In order to ensure the convergence of calculating procedure, some technical treatments like under relaxation and error feedback were adopted. The accuracy of computation, which was checked by using energy conservation of the system, was set at 0.1%.

To analyze the effect of porous materials on the thermal storage performance of the packed bed, Rock (I), Tuff and Basalt (Ma, 1986) are chosen as sample. Their physical properties are:

Rock (I): $\rho = 1400$ kg/m^3, $c = 0.836$ kJ/(kg K), $k_s = 1.74$ W/(m K)
Tuff: $\rho = 1300$ kg/m^3, $c = 0.92$ kJ/(kg K), $k_s = 0.53$ W/(m K)
Basalt (pebble): $\rho = 2695$ kg/m^3, $c = 0.92$ kJ/(kg K), $k_s = 1.71$ W/(m K).

4. Experiments

The heat storage beds with rock diameter dr = 3–4 cm and bed porosity $\theta = 0.2$–0.3, dr = 1–2 cm and $\theta = 0.1$–0.2, as well as pebble diameter dp = 3–4 cm and bed porosity $\theta = 0.2$–0.3 are selected respectively in the greenhouse. The thermal insulation was laid on the bottom of each bed. In the experiment, the floor in the heating room is insulated, instead of a heat storage bed. The temperature was measured with thermocouples, monitored by a digital voltage reader. Thermocouples are mounted on the surface and at the depth of 15 cm of heat storage bed, at the top and bottom vents of the partition wall, and in the middle of the heating room, respectively. The ambient temperature was measured with a digital thermometer. The airflow speed was measured with an anemometer. Solar radiation was measured with an actinography. All measurements were repeated more than three times for each experimental data used. A photograph of the experimental setup of the passive heating system is shown in Fig. 2.

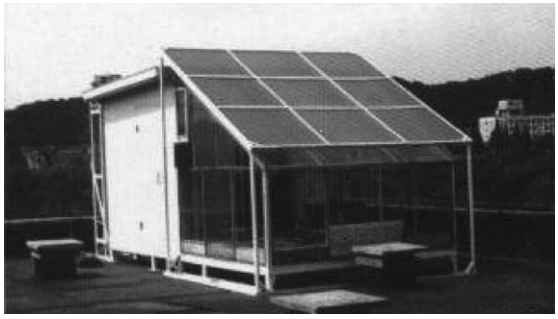

Fig. 2. Photograph of an experimental setup of passive solar heating system with a greenhouse and a heat storage layer.

5. Results and discussion

To analyze the influences of size, porosity and material of the rock bed on the capability of heat storage, we made the numerical calculation and the experiment under different rock diameters, porosities of rock bed and storage materials. The results are presented as follows.

As shown in Figs. 3 and 4, the surfaces of rock bed and partition side wall of greenhouse have comparatively higher temperature, which are the main solar absorbers in the heating system. The average air temperature inside the greenhouse is more than 20 °C above the ambient temperature. As the heat exchange occurs between the glass enclosures and the ambient, air temperature near the glass wall of enclosure inside the greenhouse is lower, in contrast, air temperature near the upper vent of the partition wall is higher. The farther the position from the upper vent in the heating room is, the lower the air temperature is. Air temperatures near north wall, floor and bottom vent in the heating room are also relatively lower. As the air in the greenhouse is heated, its temperature rises upward, and the heated air goes through the top vent into the heating room. Then the air with relatively lower temperature in the heating room goes through the bottom vent into the greenhouse to be heated again. It forms a cycle of airflow in the heating system. The average air temperature

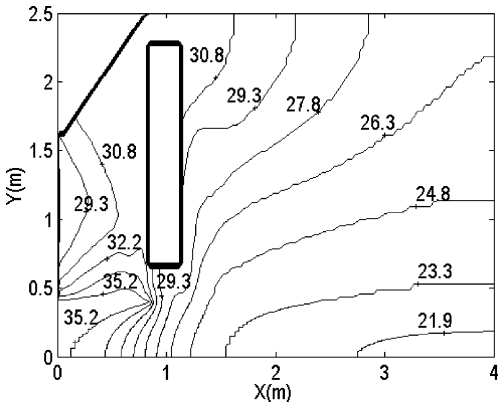

Fig. 3. Isotherms (°C) in the solar heated system with an insulated north wall, rock diameter of 4 cm and rock-bed porosity of 0.25.

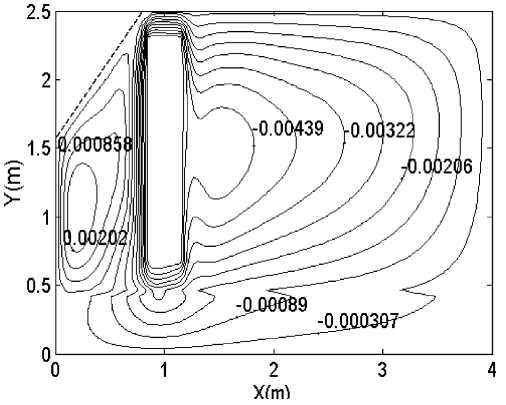

Fig. 4. Streamlines in the solar heating system with an insulated north wall, rock diameter of 4 cm and rock-bed porosity of 0.25.

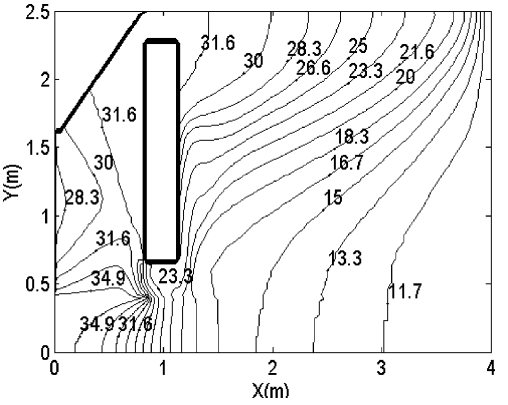

Fig. 5. Isotherms (°C) in the solar heating system with an uninsulated north wall, rock diameter of 4 cm and rock-bed porosity of 0.25.

in the heating room is nearly 10 °C above the ambient temperature, which meets the need for heating. For the temperature distribution in the rock bed, we find the temperature of bed in the greenhouse is higher. Thus, if there is no sunlight available during daytime or at night, the heated rock bed will release heat to raise the air temperature in the greenhouse.

The temperature difference causes the airflow cycle in the heating room. The surface temperature of the partition side wall of greenhouse has great effects on the temperature distribution and the airflow in the heating room, so the solar radiant absorptance of partition wall surface should be increased to enhance the heating effect. The solar radiation absorbed by the heat storage layer mainly causes the airflow cycle in the greenhouse. There is a great temperature difference between the heat storage layer in the greenhouse and the air at the bottom vent on side of heating room, so that the airflow in the system is very intensive.

As shown in Figs. 5 and 6, as the north wall of the heating room has not been insulated thermally in this case, the heat loss through the north wall occurs. There are clearly two air circulations in the heating room. Since the inner surface of north wall tends to be cooler than the other surfaces, heat is drawn from the air in the room through this surface to the ambient. The cooled air tends to sink down, while the warmer air at the top of the heating room flows in to take its place, which is the way of air movement in the heating room, so that the heat loss from the air in the room to the outside is intensified too.

Comparison between Figs. 3 and 4 and Figs. 7 and 8 can show that the effect of rock size on temperature distribution and airflow inside the rock bed is significant. Within the rock bed of $dr = 2.5$ cm and $\theta = 0.25$, the airflow is slight comparatively and the heat exchange occurs mainly in the way of heat conduction. With in-

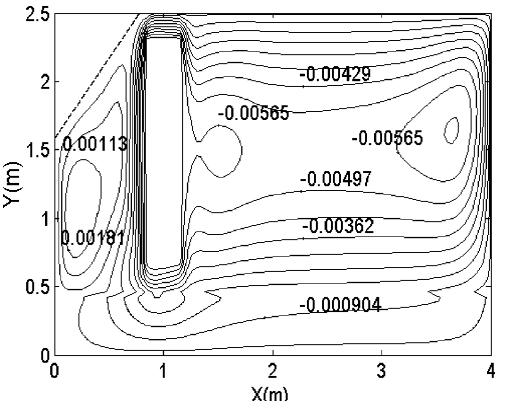

Fig. 6. Streamlines in the solar heating system with an uninsulated north wall, rock diameter of 4 cm and rock-bed porosity of 0.25.

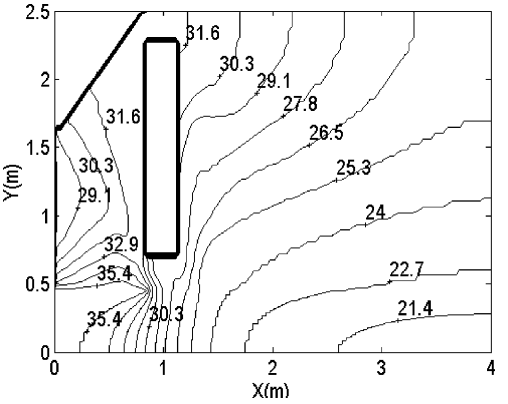

Fig. 7. Isotherms (°C) in the solar heating system with an insulated north wall, rock diameter of 2.5 cm and rock-bed porosity of 0.25.

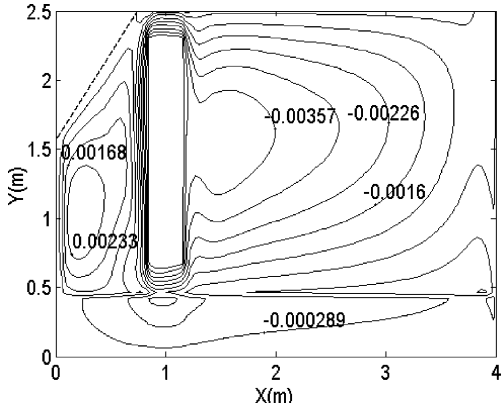

Fig. 8. Streamlines in the solar heating system with an insulated north wall, rock diameter of 2.5 cm and rock-bed porosity of 0.25.

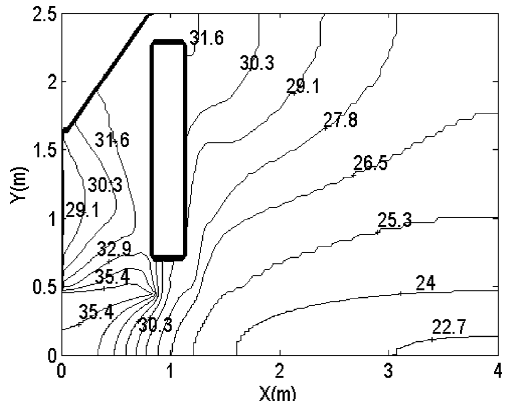

Fig. 10. Isotherms (°C) in the solar heating system with an insulated north wall, rock diameter of 2.5 cm and rock-bed porosity of 0.4.

crease in rock diameter from 2.5 to 4 cm at $\theta = 0.25$, heat convection in the rock bed increases, and it can be seen that the temperature of rock bed near the north wall of heating room rises obviously. Fig. 9 also shows that the average temperature of rock bed rises with increase in rock diameter at a constant porosity of bed. Energy stored in the rock bed increases in this case.

Comparison between Figs. 7 and 8 and Figs. 10 and 11 shows that the increase in the bed porosity from 0.25 to 0.4 at the same rock size during the heating results in an increased temperature of the rock bed near the north wall of the heating room. In this case, apparent thermal conductivity decreases with an increase in porosity, but more fluid flows into the rock bed. As a result, heat convection between the air inside the heating room and the rock bed is intensified, and the average temperature of the bed rises (see Fig. 12). However, with increase in the bed porosity for the same bed volume, rock mass and energy storage capability of the bed decreases. So,

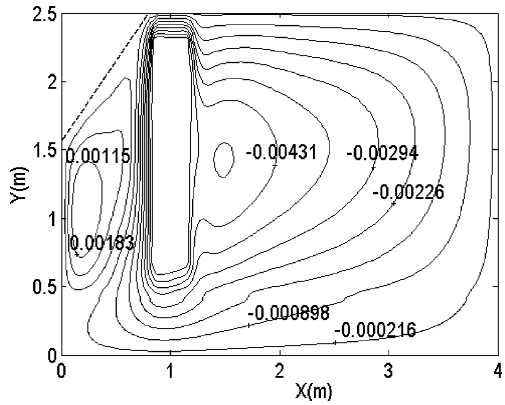

Fig. 11. Streamlines in the solar heating system with an insulated north wall, rock diameter of 2.5 cm and rock-bed porosity of 0.4.

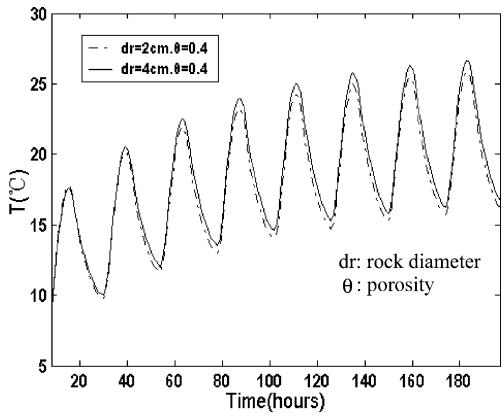

Fig. 9. Average temperature change versus time for various rock diameters of the bed at bottom of the heating system.

both bed temperature and rock mass in the heat storage layer should be in consideration with an increase in the bed porosity.

The experimental data of temperature variations of the rock bed on the surface and at depth of 15 cm for different rock sizes and porosities are shown in Fig. 13. It reveals that due to increasing in solar radiation, the temperature on bed surface became higher than that at depth of 15 cm below the surface. When solar radiation was not available, the temperature at depth of 15 cm became higher contrarily. Temperature comparison for rock beds with dr = 3–4 cm, $\theta = 0.2$–0.25 and dr = 1–2 cm, $\theta = 0.1$–0.15 shows that the surface temperatures of the two rock beds tended to be equal when solar radiation existed, but at depth of 15 cm below the surface, the temperature of rock bed with dr = 1–2 cm and $\theta = 0.1$–0.15 was lower. However, when solar radiation was not available, there was slight temperature differ-

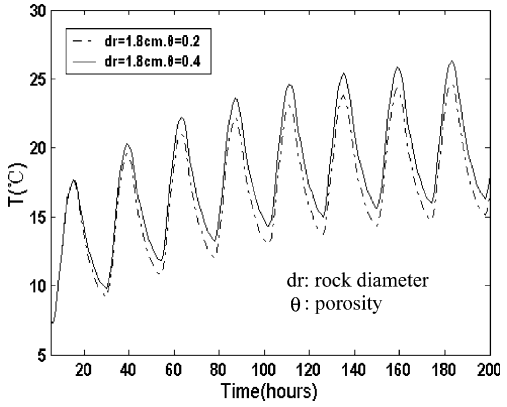

Fig. 12. Average temperature change versus time for various porosities of the bed at bottom of the heating system.

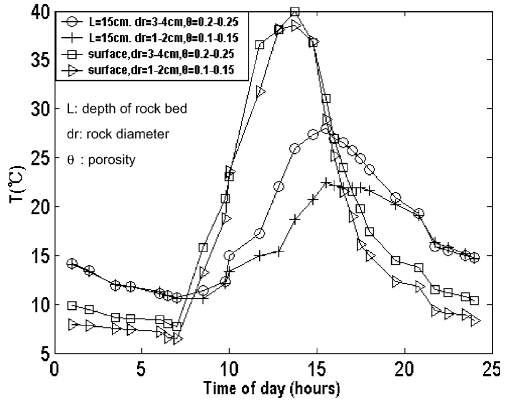

Fig. 13. Hourly mean values of temperature measured on bed surface and at 15 cm of rock bed (dr = 3–4 cm, $\theta = 0.2$–0.25) and rock bed (dr = 1–2 cm, $\theta = 0.1$–0.15) in the greenhouse, from 25–26 of November 2002, in Wuhan, China.

ence between the two beds at depth of 15 cm, but the surface temperature of the rock bed with dr = 3–4 cm and $\theta = 0.2$–0.25 was higher than that of the rock bed with dr = 1–2 cm and $\theta = 0.1$–0.15. With an increase in rock size and void fraction of the bed, heat convection and airflow within the rock bed were intensified. As a result, during the heating period, more energy was gained in the rock bed and the average temperature of bed rose, so that more heat stored in the bed could be released to the room when solar radiation was not available.

From the numerical and the experimental results (see Figs. 9, 12 and 13), we can see that due to the variation of solar radiation intensity, the temperature difference between the two beds with different porosity and rock size changed with time. However, the temperature of the rock bed with larger porosity and rock size was relatively higher. So, with increase in rock size and porosity of rock bed in a proper range, the temperature of thermal storage bed and the effect of thermal storage will increase.

Temperature variation in the rock bed with time for different depth is presented in Fig. 14. The peak temperature of rock bed moves inside after 2 p.m. in the afternoon. The temperature at the depth of 0.45 cm in the rock bed increases with time until 8 p.m. at night. Afterwards, it increases slightly and is more than 10 °C above the surface temperature of bed. So, the rock bed releases heat to raise the temperature of the heating system.

Comparison between the experimental and the numerical results (see Figs. 13 and 14) shows that due to the decrease in solar radiation, the peak temperature moved into the rock bed versus time, and with the increase in depth, the temperature of the rock bed rises to a relatively higher level. Thus, heat is stored in the rock bed for later use.

Fig. 15 shows that the average temperatures of different heat storage materials change versus time for Rock (I), Tuff and Basalt, which have the typical characteristics for thermal storage. It is clear that the averages temperature of bed increases when the Tuff with lower thermal conductivity is used. With increase in the specific heat capacity (ρc) of rock, the average temperature of bed decreases greatly when the sun is shining. However, when the sun is not shining, the average temperature of bed with lower (ρc) value is slightly higher than that with higher (ρc) value. Therefore, thermal conductivity and specific heat capacity (ρc) of the rock play an important role in the heat storage.

The temperatures were measured on the surface and at depth of 15 cm of the Rock (I) and the Basalt (pebble) beds over a day shown in Fig. 16. The specific heat capacity (ρc) of Rock (I) is lower than that of pebble, and there is slight difference in thermal conductivity between Rock (I) and pebble. Though the surface of pebble bed had higher temperature, the temperature of

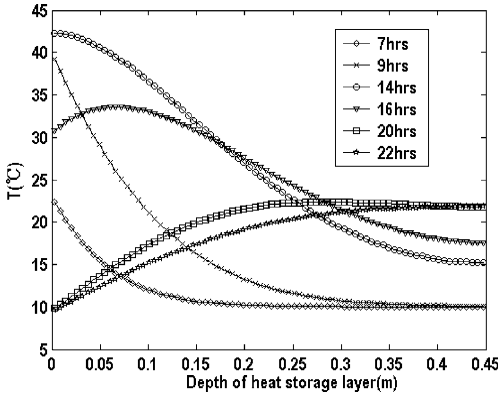

Fig. 14. Temperature distribution in the rock bed (dr = 4 cm, $\theta = 0.25$) in a day.

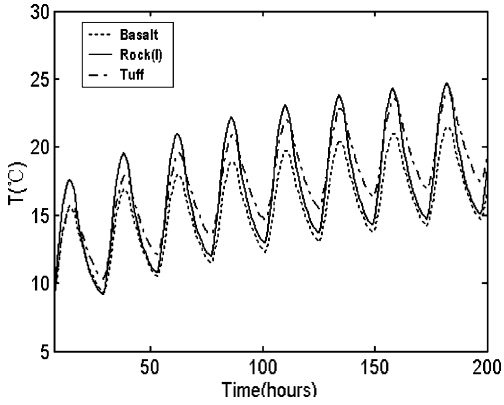

Fig. 15. Average temperature change versus time for various material of rock bed worked as a heat storage layer at bottom of the heating system.

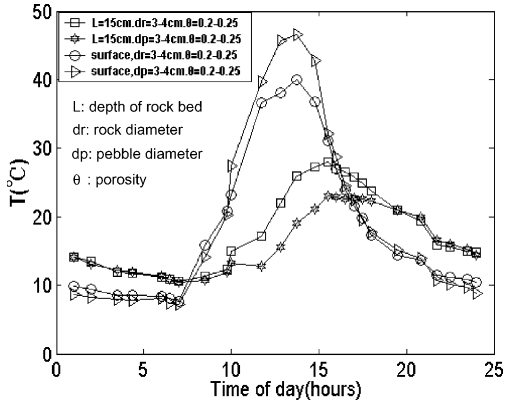

Fig. 16. Hourly mean values of temperature measured on surface and at 15 cm of rock bed (dr = 3–4 cm, $\theta = 0.2$–0.25), and of pebble bed (dp = 3–4 cm, $\theta = 0.2$–0.25) in the greenhouse, from 25–26 of November 2002, in Wuhan, China.

Rock (I) bed at depth of 15 cm was higher relatively when the sun is shining. With decrease in the solar radiant intensity, the temperature of Rock (I) bed at depth of 15 cm reduced more than that of pebble bed. In general, however, the temperature difference was small between the Rock (I) bed and the pebble bed on the surface and at depth of 15 cm when no solar irradiation was available.

Figs. 15 and 16 show that the temperature of the rock bed with lower specific heat capacities (ρc) varied more greatly versus time and was higher relatively in the periods of the solar radiation. Due to the decrease in solar radiation, the temperature difference between the heat storage beds reduced, which have difference specific heat capacities (ρc). For the effects of bed materials with different specific heat capacities (ρc) on the temperature of the heat storage bed, the results obtained from the numerical analysis are consistent with those gained from the experiments.

As shown in Fig. 17, it can be seen that from the top vent to the bottom vent in the heating room, the measured temperature went down during the heating period, corresponding with the numerical results (see Figs. 3, 7 and 10). As no heat storage layer located below the floor of the heating room, the air temperature near the floor was always lower. Fig. 18 shows that during the heating period, the temperature of greenhouse was more than 20 °C above the ambient temperature during daytime, but when the solar radiation was not available, there was slight difference between the air temperature inside the greenhouse and the ambient temperature outside the greenhouse.

Additionally, for a better design of the passive solar heating system, dampers should be set both at the top vent and the bottom vent to open or block off the air circula-

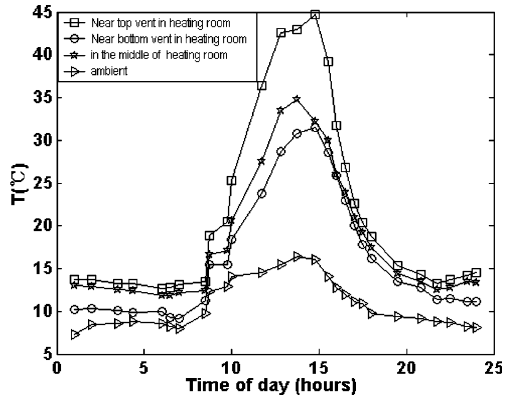

Fig. 17. Ambient temperature and air temperatures measured near top vent, bottom vent and in middle of heating room, from 25–26 of November 2002, in Wuhan, China.

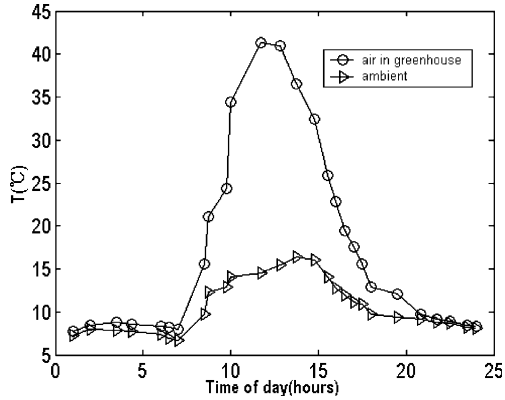

Fig. 18. Ambient temperature and temperature measured in middle of greenhouse, from 25–26 of November 2002, in Wuhan, China.

tion between the heating room and the greenhouse. So unwanted solar energy supply in the summer is limited and the reverse circulation is forbidden in the operation.

6. Conclusion

From the above discussions, we can conclude that the temperature of the solar heating room with a greenhouse and a heat storage layer can rise up more than 10 °C above ambient temperature in winter, so the energy consumption of the system can be reduced due to utilization of solar energy. Numerical results show that the wall thermal insulation of solar heating room has great effects on temperature distribution and gas flow in the heated space. The walls of heating room should be well insulated, and the solar absorptance of the partition wall surface on the greenhouse side should be increased to enhance the heating effect. Heat absorption, storage and insulation are the main factors in this solar heating system. The numerical and experimental results indicate that keeping the rock-bed porosity at certain value, an increase in rock size causes an increase in temperature, heat storage capability of rock bed, and heating effect. Additionally, keeping rock size and bed volume at certain value, an increase in porosity causes the bed temperature to rise, but rock mass in the bed to decrease. The specific heat capacities (ρc) and thermal conductivity k_s have remarkable effect on the average temperature of the rock bed in the heating system. The mean temperature of the higher (ρc) thermal storage rock bed is lower when the sun is shining. In contrast, the lower k_s thermal storage rock bed k_s has higher temperature when the sun is not shining. Therefore, when designing a rock bed as a solar absorber and a heat storage layer in the solar heating system, the rock size and bed porosity should be selected properly to raise the temperature of thermal storage bed and the effect of thermal storage.

Acknowledgements

The present study is financially supported by National Key Basic Research Development Program of China (No. G2000026303), National Natural Science Foundation of China and Doctoral Foundation of Education Ministry of China (No. 2000048731).

References

Athienitis, Andreask, 1997. Investigation of thermal performance of a passive solar building with floor radiant heating. Solar Energy 61, 337–345.

Beckermann, C., Ramadhyani, S., Viskanta, R., 1987. Natural convection flow and heat transfer between a fluid layer and a porous layer inside a rectangular enclosure. Journal of Heat Transfer 109, 363–370.

Chandra, P., Willits, D.H., 1981. Pressure drop and heat transfer characteristics of air-rock bed thermal storage system. Solar Energy 27, 547–553.

Chen, Falin, Chen, C.F., 1992. Convection in superposed fluid and porous layers. Journal of Fluid Mechanics 234, 97–119.

Chen, Shang-Mo, 1990. Heat Transfer. High Education Press, Beijing. pp. 341–344.

Choudhury, C., Chauhan, P.M., Garg, H.P., 1995. Economic design of a rock bed storage device for storing solar thermal energy. Solar Energy 55, 29–37.

Coutier, J.P., Farber, E.A., 1982. Two application of numerical approach heat transfer process within rock beds. Solar Energy 29, 451–462.

Dickinson, William C., Anderson, Bruce N., 1980. Solar Energy Technology Handbook. New York, pp. 130–131.

Duffie, J.A., Beckman, W.A., 1980. Solar Engineering of Thermal Processes. Wiley, New York.

Ergun, 1952. Fluid flow through packed columns. Chemical Engineering Progress 48, 89–92.

Iacovides, H., Raisee, M., 2001. Computation of flow and heat transfer in two-dimensional rib-roughened passages, using low-Reynolds-number turbulence models. International Journal of Numerical Methods for Heat & Fluid Flow 11, 138–155.

Kang, Shao-Zhong, 1992. Computer simulation of water transport in soil-plant-atmosphere continuum. Shui Li Xue Bao 3, 1–12.

Ma, Qing-Fang, 1986. Practical Thermal Physical Property Handbook. The Chinese Agriculture Mechanics Press, Beijing. pp. 701–710.

Neale, G., Nader, W., 1974. Practical significance of Brinkman's extension of Darcy's law. Canadian Journal of Chemical Engineering 53, 475–478.

Nisbet, S.K., Kwan, C.M., 1987. The application of the transwall to horticultural glasshouses. Solar Energy 39, 473–487.

Patankar, S.V., 1980. Numerical Heat Transfer and Fluid Flow. Hemisphere Publishing Corp, New York.

Raman, P., Mande, Sanjay, 2001. A passive solar system for thermal comfort conditioning of buildings in composite climates. Solar Energy 70, 319–329.

Rees, D.A.S., 2002. The onset of Dary–Brinkman convection in a porous layer: An asymptotic analysis. International Journal of Heat and Mass Transfer 45, 2213–2220.

Robinson, Jeremy, Dorenkamp, Angela, 1977. Solar Energy: Fundamentals in Building Design. Total Environmental Action Press. p. 141.

Tao, Wen-Quan, 2001. Numerical Heat Transfer, second ed. Xi'an Jiaotong University Press, Xi'an. pp. 329–385.

Yang, Hongxing, Zhu, Zuojin, Burmett, Joho, 2000. Simulation of the behaviour of transparent insulation materials in buildings in northern China. Applied Energy 67, 293–306.

Zhang, Suning, 1997. The institution of the hourly solar radiation model. Acta Energiae Solaris Sinica 18, 273–277.